BABEŞ-BOLYAI" UNIVERSITY CLUJ-NAPOCA

FACULTY OF PHYSICS

BIOPHYSICS AND MEDICAL PHYSICS SPECIALIZATION

MASTER'S THESIS

Scientific coordinator

Prof. dr. Nicolae Leopold

Lect. dr. Ştefania-Dana Iancu

Graduate

Georgiana Ion

2025

"BABEŞ-BOLYAI" UNIVERSITY CLUJ-NAPOCA

FACULTY OF PHYSICS

BIOPHYSICS AND MEDICAL PHYSICS SPECIALIZATION

MASTER'S THESIS

Optimization of SERS detection of anionic and cationic compounds of biomedical interest

Scientific Coordinator

Prof. dr. Nicolae Leopold

Lect. Dr. Ştefania-Dana Iancu

Graduate

Georgiana Ion

2025

Table of Contents

Introduction 5
1 Theoretical background 7
1.1 Raman effect 7
1.2 Surface-Enhanced Raman Spectroscopy (SERS) 10
1.3 The role of halide ions in the SERS detection of cationic compounds 12
1.4 The role of cations in the SERS detection of cationic molecules 12
1.5 Development of a Surfactant-Free SERS Substrate 14
2 Experimental methods 15
2.1 Silver nanoparticle colloids synthesis and characterization 15
2.2 Preparation of dried substrates 15
2.3 Raman and SERS measurements 17
3 Results and discussion 19
3.1 UV-Vis spectra 19
3.2 Selective analyte detection on colloidal substrate 20
3.3 Effect of Ca^{2+} inactivated by drying the nanoparticles 22
3.4 Employing Ca^{2+} ions for developing selective dry substrates 24
3.4.1 cit-AgNPs@Ca^{2+} for anionic analyte detection 24
3.4.2 hya-AgNPs@Ca^{2+} for cationic analyte detection 25
3.5 Surfactant-Free SERS substrate 27
3.6 Optimized SERS detection on a urine sample 28
Conclusions 30

Introduction

A current trend in scientific and technological innovation is the shift from macro- to the nanoscale, enabling the development of portable and efficient tools, that are cost-effective and require fewer production materials. This transition to nanotechnologies is especially important in substance analysis, where it is essential for the analytical method to correctly identify trace concentrations of analytes, that often go undetected by conventional methods.

Surface-enhanced Raman spectroscopy (SERS) is a technique that enables ultrasensitive measurements, with detection limits in the nanomolar range and, under optimal conditions, even down to the single-molecule level (sm-SERS) [1]–[3]. As a fast, non-invasive and non-destructive technique, SERS has demonstrated significant potential across a wide range of applications. For example, it has been used to detect environmental contaminants such as pesticides and heavy metals, where classical analytical methods require either complex sample preparation or costly, time-consuming instrumentation [4], [5].

Furthermore, literature highlights the potential of SERS in medical screening through biomarker identification and classification of various pathologies, including different types of cancer (with reported accuracies ranging from 80% to 100%) [6], autoimmune diseases (over 90%) [7], and osteoarthritis (100%) [8].

Despite its proven potential, SERS remains limited by the lack of a standardized and controlled measurement protocol. A universal substrate is unlikely to exist due to the wide variety of target analytes. Moreover, literature lacks systematic and comparative studies on optimizing detection conditions for analytes that differ by charge.

An essential condition for obtaining SERS signal, aside from a plasmonically active substrate, is that target molecules must be near the metal surface. In the case of nanoparticles, molecules must adsorb in order to benefit from the high enhancement factors. However, nanoparticles in suspension are typically coated with negatively charged surfactants. Upon analyte addition, adsorption occurs competitively: depending on electrostatic repulsion and analyte–substrate affinity, adsorption can be hindered by the surfactant.

These intrinsic limitations can be modified by the presence of specific ions, which promote the adsorption of analytes that are otherwise difficult to detect [9]. In fact,

the selective SERS detection of anionic and cationic molecules promoted by atomic ions was proved in colloidal solution up to the single molecule level [3]. We investigated whether this effect could also be useful for creating a selective solid substrate. Beyond colloidal solutions, the SERS signal can also be obtained by drying nanoparticles on a planar surface (such as glass slides) to form a solid substrate. This detection method is simplified, requiring only addition of the analyte onto the substrate followed by direct spectrum acquisition ("drop & detect"). For this reason, the method is suitable for integration into lab-on-a-chip systems for on-site testing (Point of Care testing) [10].

This study aims to develop selective, solid-phase silver SERS substrates (one aimed at cationic and the other at anionic detection) for biomedical applications, specifically in translating SERS methodology into a medical screening tool. The influence of the surfactant (citrate, chloride), the aggregation state of the silver substrate (in solution or dried), and the role of atomic ions will be evaluated in the context of label-free, selective molecular detection.

Additionally, developing a surfactant-free SERS substrate can enable adsorption of compounds with weaker affinity than that of the surfactants [11]. The study also aims to optimize a method for obtaining a solid SERS substrate without a surfactant, to overcome detection limitations imposed by surfactants.

Lastly, the performance of the optimized substrate was evaluated using a real urine sample from a patient, under varying dilution and pH conditions, to assess its applicability in a clinical setting.

The results of this master's thesis have been presented as part of the following conferences:

87th Annual Meeting of DPG and DPG-Frühjahrstagung of the Condensed Matter Section (SKM), Berlin, 2024;

20th International Conference „Students for Students", Cluj-Napoca, 2024;

18th National Conference of Biophysics, Iaşi, 2024;

88th Annual Meeting of DPG and DPG-Frühjahrstagung of the Condensed Matter Section (SKM), Regensburg, 2025.

1 Theoretical background

1.1 Raman effect

A rapid, non-destructive way to identify molecules is through spectroscopies based on visible or near-IR light, such as Raman scattering.

One of the phenomena of light interacting with molecules is scattering. The description follows the classical framework outlined by Long (2002) [12]. Consider the interaction between a single photon and a molecule. The incident photon has the angular frequency ω_1 with the corresponding energy $\hbar\omega_1$. In contrast to absorption, a scattered photon has a lower energy than that required for absorption (and thus electronic transition in the molecule) to take place. Thus, the photon is scattered, which can be viewed as a process of instant annihilation of the photon $\hbar\omega_1$ and the creation of another photon of $\hbar\omega_s$, where ω_s is the angular frequency of the scattered photon. The energy (or rather, energy shifts) of this scattered photon is what gives us crucial information about the molecule.

If the energy of the scattered photon remains the same as for the incident photon, such that $\hbar\omega_s = \hbar\omega_1$, the effect is called elastic scattering or Rayleigh scattering (Figure 1-1). But because of the scattered light being of the same energy, it does not contain any information about the molecular structure of the sample.

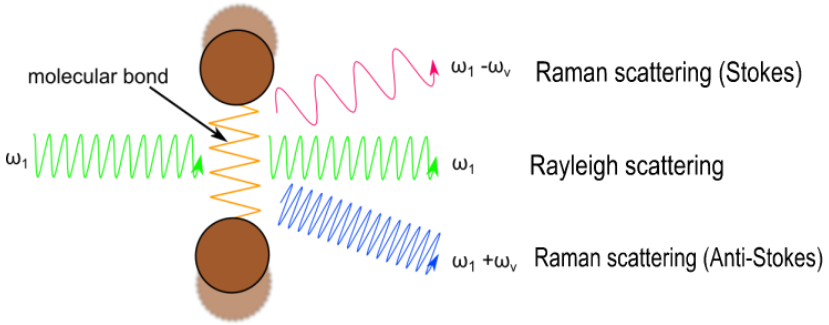

Figure 1-1. Schematic representation of Rayleigh, Stokes, and anti-Stokes scattering. An incident photon (green) interacts with a molecule. In Rayleigh scattering (center), the scattered photon has the same energy. In Stokes scattering (pink), the scattered photon has lower energy due to excitation of a vibrational mode. In anti-Stokes scattering (blue), the scattered photon has higher energy as the molecule transitions to a lower vibrational state. Adapted from https://www.physik.uni-bielefeld.de/biopho/index.php/en//index.php?option=com_content&view=category&id=21&Itemid=83&lang=en.

The energy of the scattered photon could also differ from the energy of the initial one ($\omega 1 \neq \omega s$). This effect is called **Raman scattering**, discovered by Sir C.V. Raman in 1928 during experiments on scattered sunlight in liquids.

If the scattered photon is of lower energy than the incident photon, which is the case for the experiment done by Raman, the effect is called **Raman Stokes scattering**. The scattered photon could also have a higher energy than the incident one, in which case the effect is termed **anti-Stokes Raman scattering**.

A model for better understanding the Raman Stokes scattering is depicted in Figure 1-2.A. The molecule involved in the scattering process is described by an initial state of energy E_i and a final state E_f, where E_i and E_f represent different vibrational modes of the ground electronic state E_g. When a photon is annihilated, the effect can be considered a virtual absorption, with the molecule being excited to a virtual state. If Raman scattering takes place, the molecule returns to a different vibrational level within the ground electronic state, namely E_f. Because overall the conservation of energy must take place, the difference in energy of both vibrational modes will be equal to the difference in energy between the scattered and the incident photon, $\Delta E = \hbar(\omega_1 - \omega_s)$. For example, during scattering, the molecule could be excited from the vibrational ground state v=0 to the first excited vibrational state v=1 (see Figure 1-2.B.). This energy corresponds to a certain vibrational mode of the studied molecule. As Raman spectroscopy is able to measure the exact energy of the inelastically scattered light over a chosen spectral range, it can give information about the vibrational modes (and thus the molecular structure) of the analyte of interest.

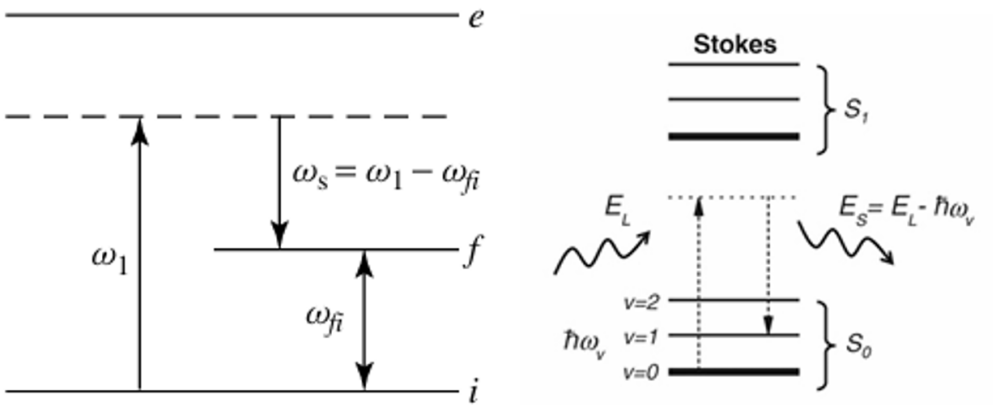

Figure 1-2. Energy-level diagrams illustrating the Raman scattering process. Left: A photon of energy $\hbar\omega_1$ excites the molecule to a virtual state and is scattered with a smaller energy energy (ω_s) corresponding to a vibrational transition (ω_{fi}). Adapted from Long (2002) [12]. Right: Vibrational levels within electronic states show the origin of Stokes scattering ($E_S=E_L-\hbar\omega_v$), with the transition starting from the ground vibrational level. Adapted from Le Ru, E. C., & Etchegoin, P. G. (2009) [2].

A more detailed analysis of the scattering mechanism reveals why some vibrational modes are Raman active while others aren't.

The classical approach considers light scattering to be a consequence of the oscillating electric dipole induced in a molecule by the electromagnetic (EM) field of the incident light wave.

Such an oscillating electric dipole will emit electromagnetic radiation of intensity I in a direction making an angle θ with the orientation of the induced dipole:

$$I = k'_{\omega}\omega_s^4 p_0^2 sin^2\theta \quad (1)$$

where k_ω' is a constant, ω_s is the frequency of the induced electric dipole, p_o is the induced electric dipole moment determined by the properties of the molecule and the incident radiation ω_1. The induced electric dipole moment can be expressed as a rapidly converging series of vectors:

$$p = p^{(1)} + p^{(2)} + p^{(3)} + \cdots \quad (2)$$

with the first term being linear in E. $p^{(1)}$ has three frequency components: one for Rayleigh scattering and the other two for Raman scattering (Stokes and anti-Stokes):

$$p_0(\omega_1) = a^{Rayleigh} E_0(\omega_1) \quad (3)$$

$$p_0(\omega_1 \pm \omega_k) = \alpha^{Raman}\, E_0(\omega_1) \quad (4)$$

where $p_0(\omega_1)$ and $p_0(\omega_1 \pm \omega_k)$ are time-dependent induced dipole moments at the oscillating frequencies of ω_1 and $\omega_1 \pm \omega_k$. α is the polarizability tensor of the molecule and describes how the molecule's electron cloud deforms in response to an external electric field.

For Raman scattering, the produced electric field will have a different frequency than the initial electric field. For this to happen, the induced dipole moment must be oscillating at the frequency $\omega_1 \pm \omega_k$, which means that the molecule produces an additional modulation of frequency ω_k. As shown in Eq. (4), because the initial electric field E_o remains constant, the modulation of the frequency of oscillation is caused by a change in the polarizability tensor. The condition for Raman scattering is to have a change in the polarizability with respect to the change in vibrational coordinate, Q [13]:

$$\left(\frac{\partial \alpha}{\partial Q}\right) \neq 0 \qquad (5)$$

Eq. (5) indicates that not all vibrational modes will be Raman active, but only the ones that are characterized by a change in polarizability with position.

This leads to the expression of the intensity of Raman scattered radiation:

$$I_R \propto v^4 I_0 N (\frac{\partial \alpha}{\partial Q})^2 \qquad (6)$$

Where I_0 is the initial radiation intensity, N is the number of scattering molecules, $v = \omega/2\pi$ is the frequency of the initial radiation, and $(\frac{\partial \alpha}{\partial Q})$ is the change in polarizability with vibrational amplitude.

1.2 Surface-Enhanced Raman Spectroscopy (SERS)

A major limitation of implementing Raman spectroscopy in practical applications is the inherently low Raman cross-section of most compounds besides dyes. Usually, only 1 in 10^7 photons are inelastically scattered. Because Raman is a weak effect, Raman spectroscopy usually requires either high concentrations of analytes, a long acquisition time or a high laser intensity, which could result in laser-induced degradation of the sample.

The SERS effect can increase the Raman intensity up to $10^8 - 10^{10}$ times. It was first observed by Fleischmann et al., as pyridine molecules were adsorbed on roughened silver electrodes [14].

The SERS effect is explained by two distinct contributions, both of which are experimentally shown to play a role in obtaining the SERS effect: the **electromagnetic contribution** and the **chemical contribution**.

The electromagnetic contribution is based on the excitation of the local-surface plasmon resonance (LSPR) by the initial electromagnetic radiation (laser). When EM radiation interacts with metallic nanostructures, an induced oscillation of the free surface electrons takes place. The valence electron collective oscillations are quasi-particles called plasmons. When the initial EM radiation has a frequency that is in resonance with this collective electron oscillation, the local-surface plasmon resonance takes place. In this case, a large electromagnetic field is generated by the oscillating electrons in the proximity of the nanoparticle surface (see Figure 1-3 left). Molecules

that are in the vicinity of the nanoparticle benefit from the large EM field, as the Raman signal can be amplified by the intense electric field near the nanoparticles by a factor of up to 10^6-10^7 [2], with single molecule SERS events having an estimated enhancement of up to 10^{14} [15].

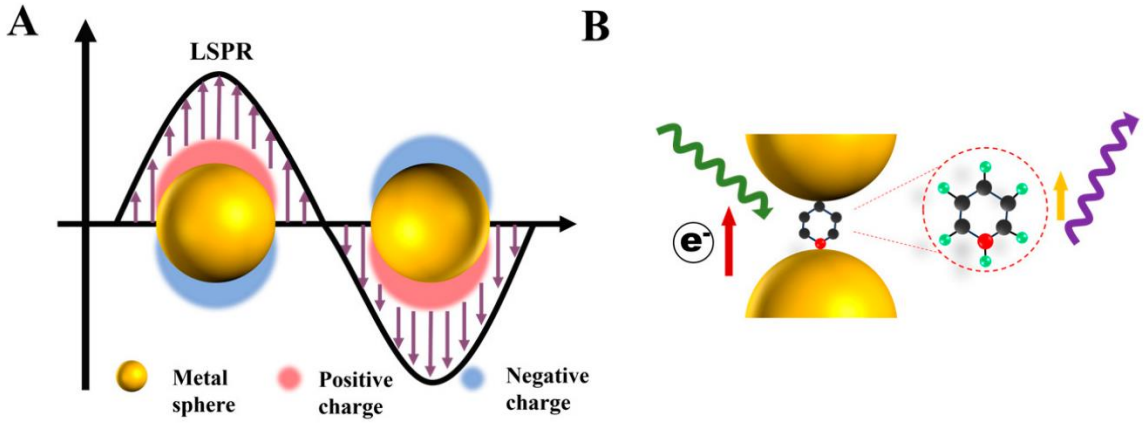

Figure 1-3 Schematic representation of the electromagnetic enhancement mechanism. Reproduced from Han, X.X., Rodriguez, R.S., Haynes, C.L. et al. *Nat Rev Methods Primers **1**, 87 (2021).*

The enhancement factor of the Stokes radiation is:

$$R = \frac{|E_{loc}|^4}{|E_0|^4} \qquad (7)$$

where E_{loc} is the local field amplitude at the active site and E_0 is the electric field amplitude of the initial radiation.

The localized EM field decays with the third power of the distance from the nanoparticle:

$$E_r = E_0 cos\theta + g\,\frac{a^3}{r^3}\,E_0 \cos\theta \qquad (8)$$

This translates to SERS enhancement being effective only when molecules are within a few nanometers of the nanoparticle surface, i.e., it is a first layer effect.

Although the electromagnetic contribution is undeniable, it cannot fully explain some experimental observations. For example, certain molecules which are known to be surrounding the nanoparticles, such as water molecules and citrate, only have minor enhancements (water molecules) or are enhanced only in very particular conditions (citrate and other surfactants) [1].

The chemical contribution complements the electromagnetic one and is based on electronic coupling and resonant charge transfer. In the presence of electromagnetic radiation, electrons from the nanoparticle perform a transition from the Fermi level of the metal substrate to the LUMO level of the chemisorbed molecule. When the electron relaxes back to its initial state, the molecule may remain in an excited vibrational state, resulting in Raman signal amplification by several orders of magnitude [16].

1.3 The role of halide ions in the SERS detection of cationic compounds

The role of ions, especially chloride ions, in enhancing the SERS signal has been extensively studied [1], [17]. In the presence of chloride, Raman signals of cationic molecules are amplified by several orders of magnitude. Until recently, all single-molecule SERS (sm-SERS) measurements reported have been conducted in the presence of chloride ions [1]. The role of halide ions in SERS enhancement goes beyond nanoparticle aggregation and hot-spot formation. This has been demonstrated through studies at sub-aggregation concentrations and on individual nanoparticles [18].

Halide anions (Cl^-, Br^-, I^-) can displace weak surfactants like citrate, chemisorb to the metal surface, and enable selective adsorption of cationic species such positive dyes [19]. Furthermore, it has been demonstrated that halide ions such as Cl- promote co-adsorption of cationic species, with Nile Blue and R6G dyes being simultaneously detected on the AgNPs@Cl^- substrate [3].

1.4 The role of cations in the SERS detection of cationic molecules

SERS detection of anions, such as carboxylate anions from carboxylic acids, is less commonly reported due to the negative surface potential of typical nanoparticle surfactants, which prevents the adsorption of anionic molecules. However, carboxylate anions – including citrate, which is usually absent in the spectrum – adsorb in the presence of cations such as Ca^{2+}, Pb^{2+}, or Al^{3+} [9].

It has been shown that the addition of divalent cations such as Ca^{2+} and Mg^{2+} facilitates the competitive adsorption of anionic species based on their binding affinity to the NPs surface. For example, adding Ca^{2+} to colloidal cit-AgNPs leads to the SERS spectrum of citrate, the capping agent. If NaCl is added to the same solution, Cl^- will desorb

citrate from the surface and the Ag-Cl^- vibration will replace the previous citrate spectrum (Figure 1-4) [19].

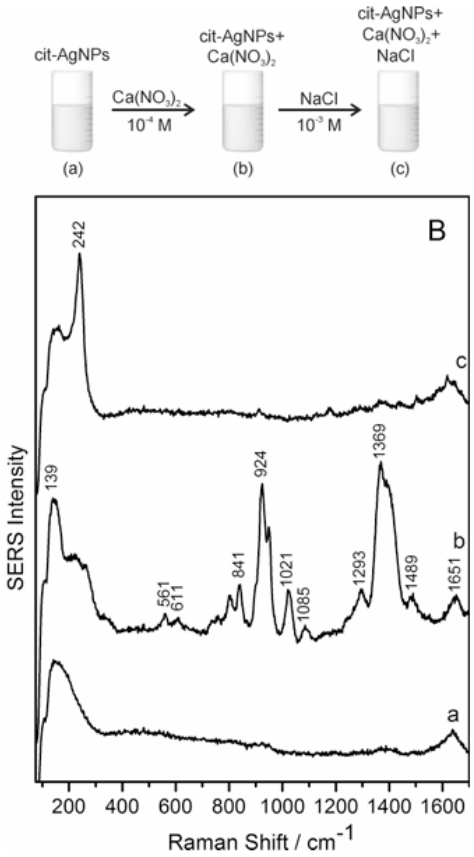

Figure 1-4 SERS active sites generation by Ca^{2+} adions and competitive chemisorption of citrate and Cl^- anions: a) Raman blank spectrum of cit-AgNPs; b) SERS spectrum of citrate obtained after activation of cit-AgNPs with Ca^{2+}; c) intense Ag-Cl^- SERS band, obtained after the replacement of citrate molecules by Cl- ions at the Ca2+ SERS active sites. Reproduced from Stefancu, A., Iancu, S.D., Moisoiu, V., Leopold N., *R.R. in Physics **70**, 509 (2018).*

Regardless of the analytes charge, studies have shown that positive ions are crucial even in the SERS detection of cationic compounds. For example, adding cations such as Ca^{2+} or Mg^{2+} promotes Cl^- adsorption, thereby, thereby generating new SERS active sites and enhancing the cationic species signal [17], [19]. This approach has enabled selective SERRS detection at the single-molecule level [3]. Mg^{2+} was used for the selective detection of the anionic dye Rose Bengal while subsequent Cl^- addition lead to the selective detection of the cationic dye R6G from the same mixture. These findings highlight the role of ionic species in facilitating selective SERS detection by mediating analyte adsorption.

1.5 Development of a Surfactant-Free SERS Substrate

A common challenge in achieving strong SERS signals is the poor affinity of many molecules for the metallic surface, which prevents them from displacing the surfactant. Moreover, strongly binding ions such as Cl^- can displace both the surfactant and adsorbed molecules. For conventional colloidal nanoparticles, however, these ions cannot be removed without altering the colloidal system, making the substrate non-reusable.

To address this, surfactant-free solid SERS substrates were proven useful for detecting low-concentration analytes (in the nanomolar range) even from vapour-phase [11], [20]. Adding cations like Fe^{3+} has also significantly increased SERS signals for compounds with inherently weak metal-surface affinity, such as neurotransmitters [20].

Various methods for preparing surfactant-free solid SERS substrates have been developed. However, many rely on costly techniques (nanolithography, vacuum deposition, laser ablation) [21] or involve agents such as HCl, whose dissociated chloride ions can interfere with SERS signal acquisition [11].

A simple alternative involves surface oxidation to strip away organic molecules followed by surface cleaning in acidic solution to eliminate the formed oxide layer. This method has been successfully applied using hydrochloric acid, although chloride interaction with silver surfaces must be considered. Other mild acidic agents, such as hydrogen peroxide (H_2O_2) could be used for oxide layer elimination.

2 Experimental methods

2.1 Silver nanoparticle colloids synthesis and characterization

AgNPs preparation by citrate reduction

All reagents were of analytical grade. Citrate-capped silver nanoparticles (cit-AgNPs) were synthesized using the Lee-Meisel method [22]. Briefly, 17 mg $AgNO_3$ were dissolved in 98 mL ultrapure water (Millipore Direct-Q3 UV) under magnetic stirring. After the solution was brought to the boiling point, 2 mL of trisodium citrate 1% were added. The solution was left to boil under stirring for 15 minutes.

AgNPs preparation by hydroxylamine hydrochloride reduction

Silver nanoparticles obtained by hydroxylamine hydrochloride reduction (hya-AgNPs) were synthesized according to Leopold-Lendl method [23]. Briefly, 17 mg of $AgNO_3$ were dissolved in 90 mL ultrapure water under magnetic stirring. Separately, 17 mg of hydroxylamine hydrochloride were dissolved in 8.8 mL of ultrapure water and 1.2 mL of NaOH 1% was added. The hydroxylamine solution was added to the $AgNO_3$ solution under stirring, and the resulting solution changed its color immediately to dark yellow. The solution was kept under stirring for another 15 minutes. Both colloidal solutions were stored at room temperature.

UV-Vis measurements

The UV-Vis spectra were acquired using a Jasco V-630 spectrophotometer with a quartz cuvette of 1 cm optical path length. For observing the effect of Ca^{2+} and Cl^-, a volume of 90 µL of NPs was mixed with either 10 µL of a $Ca(NO_3)_2$ solution to reach a final concentration of 5×10^{-4} M or with 10 µL of NaCl to reach the final concentration of 10^{-3} M. Prior to measurement, 100 µL of each resulting mixture was diluted in 1 mL of ultrapure water.

2.2 Preparation of dried substrates

Dried drop deposition

The above-mentioned cit-AgNPs colloidal solution was divided in 1.5 ml Eppendorf containers and centrifuged for 15 minutes at 7300 × *g* and 25°C. The supernatant was carefully removed, and the concentrated nanoparticles were deposited onto 20×20 mm cover glass slides. A 2 µL aliquot was applied to each slide, forming a dense silver spot as

the drop dried into a round, opaque shape, indicating a high optical density of silver nanoparticles (Figure 2-1).

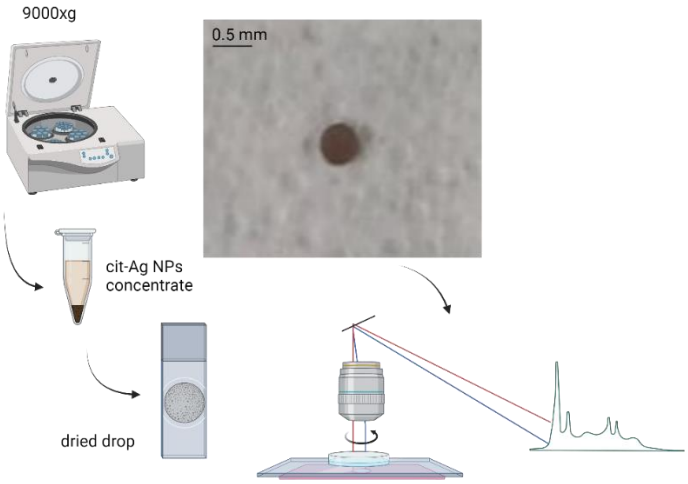

Figure 2-1 Illustration of the preparation process for the dried drop

Preparation of dried cit-AgNPs@Ca^{2+}

The synthesized cit-AgNPs colloid was divided in 1.5 ml Eppendorf containers and mixed with 1.5 ml $Ca(NO_3)_2$ 10^{-1} M (final concentration of 10^{-4} M) prior to centrifugation. No nanoparticle aggregation was observed in the presence of 5×10^{-4} M $Ca(NO_3)_2$, as confirmed by the UV-Vis spectra, which demonstrated the stability of the colloidal nanoparticle solution. The solution was centrifuged for 15 minutes at 7300xg and at 25°C. The supernatant was removed and the concentrated nanoparticles (cit-AgNPs@Ca^{2+}) were left to dry for approximately 1 hour on cover glass slides in drops of 2 μl each.

Preparation of dried hya-AgNPs@Ca^{2+}

The synthesized hya-AgNPs colloid was divided in 1.5 ml Eppendorf containers and mixed with 1.5 ml $Ca(NO_3)_2$ 10^{-1} M (final concentration of $5x10^{-4}$ M) prior to centrifugation. The solution was centrifuged for 15 minutes at 11000 × *g* and at 25°C. The supernatant was removed and the concentrated nanoparticles (hya-AgNPs@Ca^{2+}) were left to dry on cover glass slides covered in aluminum foil tape in drops of 2 μl each.

Preparation of the surfactant-free substrate

Citrate-capped silver nanoparticles (AgNPs) were concentrated at 9000 × *g* for 15 minutes, dried on a glass slide, and exposed to an ozone-rich environment (UV Ozone Cleaner, Ossila) to eliminate the citrate surfactant, resulting in the formation of silver

oxide on the surface (AgO). To remove AgO from the surface, we tested two H_2O_2 solutions (with concentrations of 3% and 0.15%) by immersing the substrate for 70 seconds (Figure 2-2).

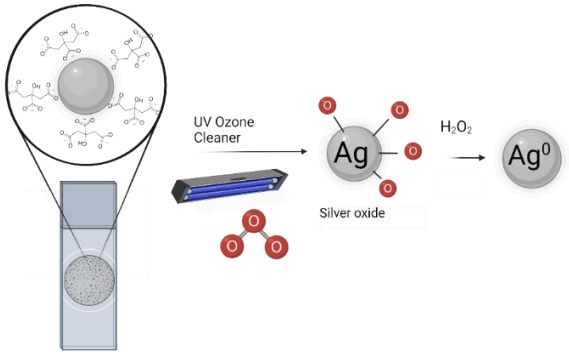

Figure 2-2 Illustration of the preparation process of surfactant free substrate

2.3 Raman and SERS measurements

All Raman/SERS measurements were recorded using a portable Raman spectrometer (iRaman 532 nm, BWTek) coupled to a microscope (BWTek) – see Figure 2-3. The spectra were recorded by focusing the laser (50 mW) through a 20x objective (NA=0.4) and averaging 3 spectral acquisitions of 5 s exposure time each. The laser intensity was set to the maximum value (100%) unless otherwise stated. The resulting spectra were then automatically processed using a Python home-built script. First, the background was subtracted, and the spectra were smoothed. Then, the intensities were normalized using vector normalization. The spectra of three prepared samples (colloidal solutions) or three different focal points from a silver spot (dried substrate) were averaged and plotted, along with their corresponding standard deviations.

Figure 2-3 Portable Raman spectrometer (iRaman 532 nm, BWTek) with built-in laser and detector (right), coupled to a BWTek microscope with a 20x objective for focusing the laser on the sample (left).

SERS measurements on colloidal substrate

The analytes were first mixed separately in an Eppendorf tube by adding equal volumes of Nile Blue A ($C_{40}H_{40}N_6O_6S$) 10^{-6} M and fumaric acid $5x10^{-3}$ M. 2 µl of this mixture is added to 100 µl colloidal cit-AgNPs. First, the SERS spectrum of the analyte mixture consisting of Nile Blue (10^{-8} M) and fumaric acid (5×10^{-5} M) was recorded. Following this, 1 µL of 10^{-1} M NaCl was added to the mixture, and the SERS spectrum in the presence of NaCl at a final concentration of 10^{-3} M was measured. Similarly, the SERS spectrum of the mixture was recorded after the addition of $Ca(NO_3)_2$ at a final concentration of 5×10^{-4} M. For the measurement, a drop of 10 µl of the sample is deposited onto an aluminum foil-covered microscope slide. Each measurement was performed three times for averaging and representation of the standard deviation.

SERS measurements on dried substrate

The solid (dried) substrate was submerged in 2 ml ultrapure water (Millipore Direct-Q3 UV) in a petri dish. Adjustments to the concentrations of Nile Blue and fumaric acid were carried out for the dried substrate to achieve the lowest concentrations that still produced clearly defined SERS bands. The analytes were first mixed separately in an Eppendorf vial by adding Nile Blue A 10^{-5} M and fumaric acid $5x10^{-3}$ M in a ratio of 10:2. Then, 12 µl of water were pipetted out of the petri dish and 12 µl of the above-mentioned mixture is added. A cover glass with 1 dried silver spot was immersed for 15 minutes in a solution containing $5x10^{-8}$ M Nile Blue and $5x10^{-6}$ M fumaric acid. The measurements were conducted while keeping the substrate submerged in the solution to avoid drying effects. Spectra were recorded from three wet spots. Next, $Ca(NO_3)_2$ was added at a final concentration of $5x10^{-4}$ M, and the SERS spectrum was measured. Similarly, NaCl at a final concentration of 10^{-3} M was added and the corresponding SERS spectra were recorded. Each measurement was performed 15 minutes after the addition of any new analyte, as this time is considered sufficient for the adsorption of the analytes or ions to the Ag surface [24].

3 Results and discussion

3.1 UV-Vis spectra

Extinction spectra were employed to assess the plasmonic properties of the silver nanoparticles. The synthesized citrate-capped silver nanoparticle (cit-AgNPs) solution exhibited a localized surface plasmon resonance (LSPR) peak at λ_{max}=424 cm^{-1}. Based on the maximum of the LSPR band, the nanoparticle diameter was estimated to be 52 nm according to established empirical relations [25].

Figure 3-1 confirms the stability of the cit-AgNPs solution after adding NaCl and $Ca(NO_3)_2$. For $Ca(NO_3)_2$ 5×10^{-4} M, the appearance of a slight shoulder at higher wavelengths suggests the onset of a small number of aggregates. However, the overall spectral profile confirms that the nanoparticles largely retain their stability in solution. For developing dried SERS substrates, the Ca^{2+} concentration was maintained well below this aggregation threshold, at 10^{-4} M. In the case of NaCl 10^{-3} M, no changes are observed in the extinction spectra, indicating that nanoparticles retain their stability.

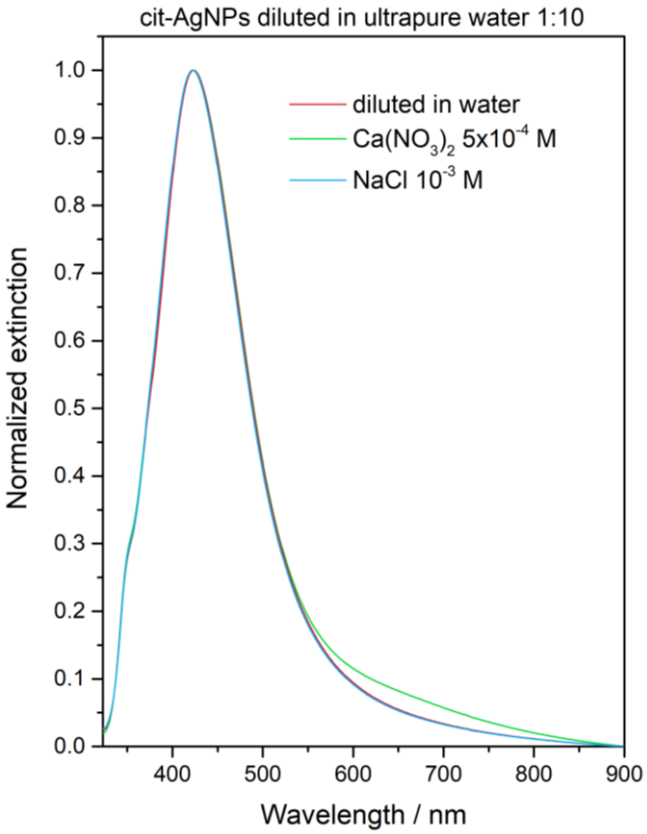

Figure 3-1 UV-Vis extinction spectra of unmodified colloidal cit-AgNPs (red) or modified with $Ca(NO_3)_2$ (green) or NaCl (blue). The colloidal solutions were diluted 1:10 in ultrapure water.

3.2 Selective analyte detection on colloidal substrate

The selective SERS detection of anionic and cationic molecules promoted by atomic ions has been first tested in colloidal solution.

Selective detection from a mixture of an anionic analyte (fumarate^{2-}) and a cationic analyte (Nile Blue) was confirmed in colloidal cit-AgNPs solution by adding Ca^{2+} and Cl^- ions. Figure 3-2 shows the SERS spectra, where the anionic and cationic species are selectively enhanced on the colloidal substrate. Citrate-capped nanoparticles in solution do not produce any detectable SERS spectra, not even from the capping agent itself, present at millimolar concentrations (a). Upon the addition of Ca^{2+} ions, the SERS peaks of negatively charged species, namely the citrate surfactant and fumarate^{2-}, are selectively enhanced. In contrast, the introduction of Cl^- ions results in the selective enhancement of only the Nile Blue signal, the positively charged analyte. These results demonstrate that atomic ions can selectively promote the adsorption of either anionic species (Ca^{2+}) or cationic species (Cl^-) on the colloidal cit-AgNPs substrate.

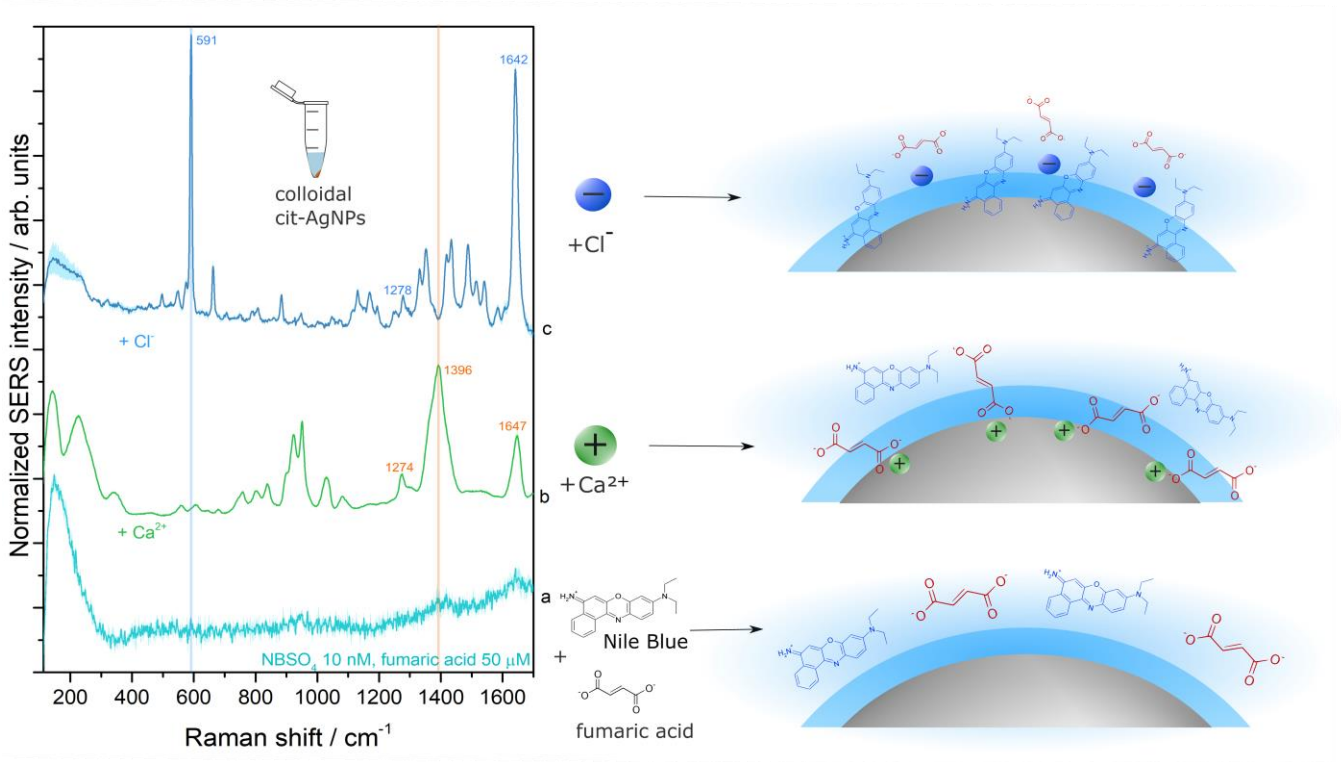

Figure 3-2 : SERS spectrum of colloidal cit-AgNPs mixed with 10 nM Nile Blue·SO_4 and 50 µM fumaric acid (a), SERS spectrum of the same mixture after the addition of 0.5 mM Ca^{2+} (b), or of 1 mM Cl^- (c)The SERS peaks corresponding to fumarate are marked with orange while peaks corresponding to Nile Blue are marked with blue.

The effect of adding both Cl^- and Ca^{2+} to the mixture was also investigated (Figure 3-3 left). In this case, Cl^- preserves its selective effect, enhancing only the cationic species. A notable difference is the appearance of the 239 cm^{-1} band in the spectrum, characteristic of the Ag-Cl vibration. Overall, tests on various colloidal cit-AgNPs batches suggest that if reproducible detection of cationic molecules is the goal, the combined addition of Cl^- and Ca^{2+} yields more consistent results compared to using Cl^- alone.

Furthermore, the effect of acidic pH on the selectivity was studied (Figure 3-3 right). The results show that lowering the pH from neutral (7) to acidic (5) by adding HNO_3 does not have a significant impact on the selective adsorption of analytes in the presence of adions.

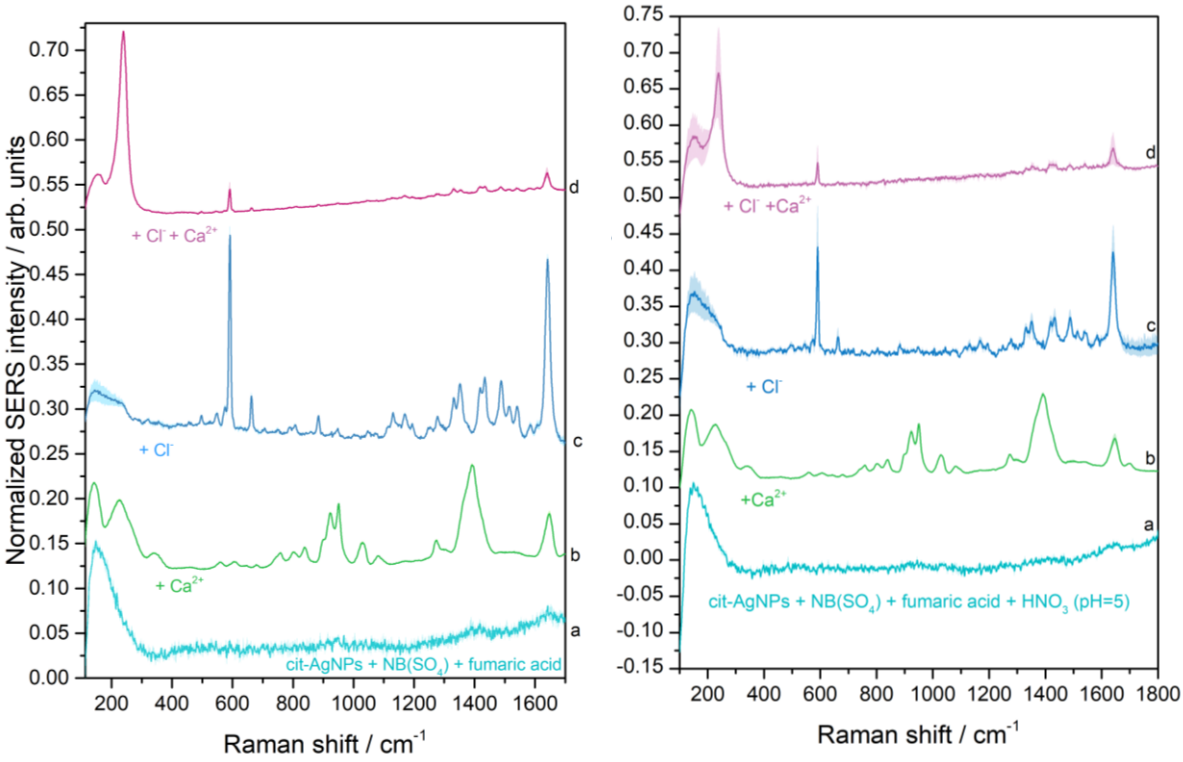

Figure 3-3 Left: SERS spectra of colloidal cit-AgNPs showed in Figure 1, mixed with 10 nM Nile Blue·SO4 and 50 µM fumaric acid (a), SERS spectrum of the solution after the addition of 0.5 mM Ca^{2+} (b), 1 mM Cl^- (c), or both (d). Right: SERS spectra of colloidal cit-AgNPs modified to have pH 5, exhibiting the same selectivity effect.

3.3 Effect of Ca^{2+} inactivated by drying the nanoparticles

Ca^{2+} has no effect when added after drying the substrate. The selective behavior of the subsequent addition of Ca^{2+} and Cl^- was also tested for a solid substrate obtained by concentrating and drying the cit-AgNPs.

The first difference compared to the colloidal substrate was the intense SERS spectrum of citrate (see Figure 3-4 left), which was chemisorbed to the Ag surface upon drying. It can be observed that citrate is chemisorbed on the Ag surface by the presence of the 232 cm^{-1} broad band, attributed to the ν(COO–Ag) vibration [24], [26]. Furthermore, after submerging the substrate in a Nile Blue and fumaric acid mixture, bands attributed to both Nile Blue (notably 592 cm^{-1}) and fumaric acid (1276, 1396, 1646 cm^{-1}) can be detected in the SERS spectrum without the addition of adions (Figure 3-4 right). Interestingly, both species adsorb spontaneously without the presence of any adion on the surface. Nile Blue is only noticeable by the presence of a weak SERS band at 592 cm^{-1}. The citrate surfactant is not completely displaced by the other analytes, as scitrate bands are still present in the spectrum (925, 948 cm^{-1}).

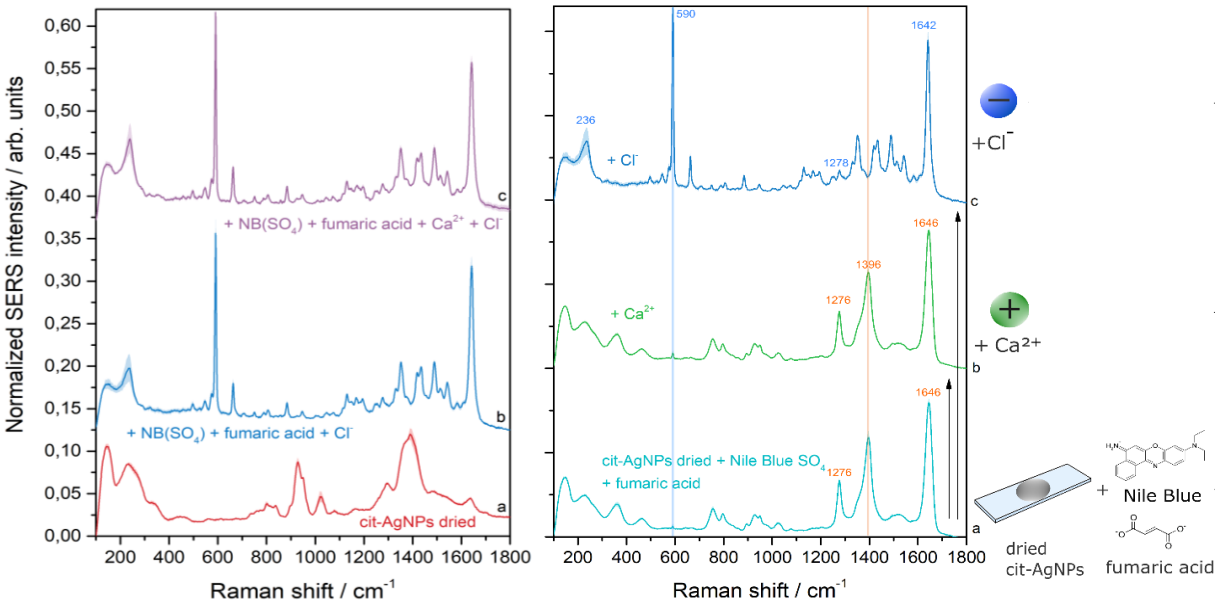

Figure 3-4 Left: SERS spectrum of a dried cit-AgNPs substrate (a), SERS spectrum of the substrate submerged in a 50 nM Nile Blue·SO_4 and 5 µM fumaric acid solution after the addition of 1 mM Cl^- (b) or of 0.5mM Ca^{2+} and 1mM Cl^- (c), showing that after drying the nanoparticles, Ca^{2+} has no effect on the signal. Right: SERS spectrum of dried cit-AgNPs substrate submerged in a 50 nM Nile Blue·SO_4 and 5 µM fumaric acid solution (a), SERS spectrum after the addition of 0.5 mM Ca^{2+} (b) or of 1 mM Cl^- (c). The SERS peaks corresponding to fumarate are marked with orange while peaks corresponding to Nile Blue (or to the Ag-Cl vibration) are marked with blue.

The addition of Cl^- adions leads to the desorption of other anionic species (fumarate, citrate), yielding an intense selective spectrum of the dye Nile Blue. A notable addition to the spectrum is the 237 cm^{-1} band attributed to the Ag–Cl^- vibration, suggesting direct adsorption of the Cl^- to the surface.

However, adding $Ca(NO_3)_2$ solution after drying the substrate did not lead to selective detection of anionic species as in the case of colloidal NPs. This suggests the addition of Ca^{2+} to the dried substrate does not promote the selective adsorption of species at the Ag surface.

These results were consistent for different cationic dyes (Nile Blue, Crystal Violet) and for different stabilizing agents (SO_4^-, Cl^-) (Figure 3-5). These findings indicate that the effect of Ca^{2+} on the selective SERS detection is hindered or inactivated by the prior drying of the substrate.

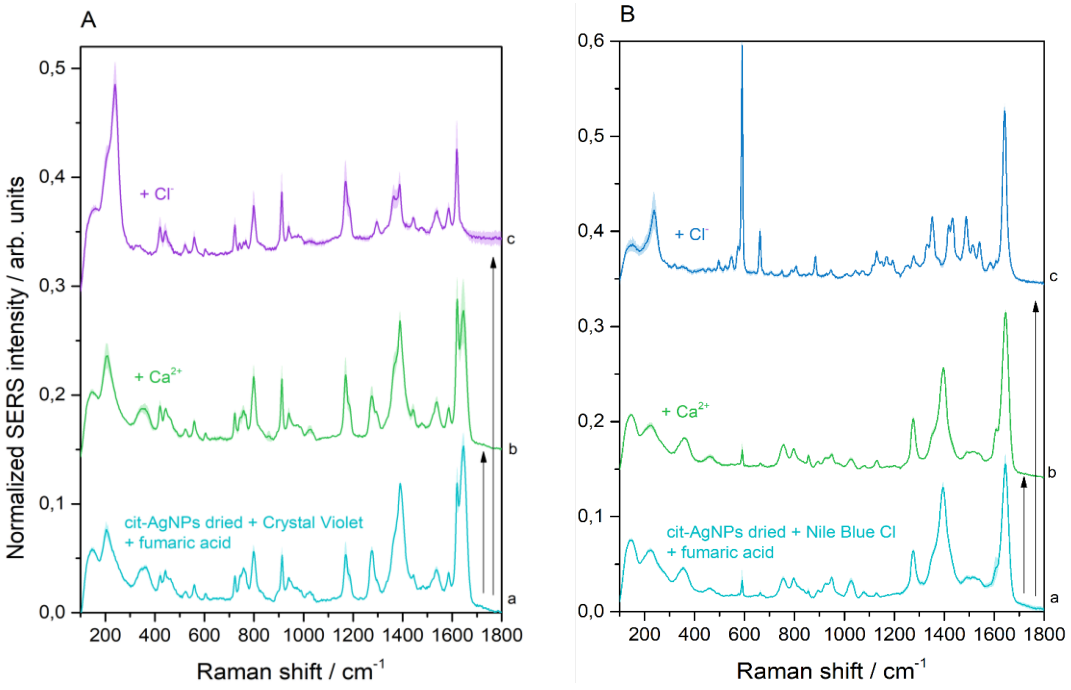

Figure 3-5 SERS spectra of dried cit-AgNPs substrates immersed in a solution of 10 mM fumaric acid and a cationic dye (a): 10 nM Crystal Violet·Cl (A) or 50 nM Nile Blue·Cl (B). SERS spectra after the addition of 0.5 mM Ca^{2+} (b) or 1 mM Cl^- (c) exhibiting similar adsorption behavior of different cationic dyes as the one presented in Figure 2. The difference in concentration for the dyes is due to the difference in Raman cross-section. The laser intensity was set at 20%.

3.4 Employing Ca^{2+} ions for developing selective dry substrates

3.4.1 cit-AgNPs@Ca^{2+} for anionic analyte detection

The addition of Ca^{2+} prior to the cit-AgNPs drying process enables the selective SERS detection of anionic or cationic analytes, respectively. Figure 3-6 presents the resulting dried substrate suitable for anionic analyte detection.

To harness Ca^{2+} capabilities of promoting the adsorption of negative species, we added the $Ca(NO_3)_2$ salt to the colloidal solution of cit-AgNPs, right before the centrifugation step. The addition of this simple step before the drying process resulted in a modified dried substrate suitable for the detection of anionic species. The dried cit-AgNPs@Ca^{2+} produce an intense SERS spectrum of citrate, indistinguishable from that obtained with plain dried cit-AgNPs (Figure 3-6 a). However, after the addition of the mixture of Nile Blue and fumarate, anionic species (fumarate and citrate) are selectively detected.

After the addition of Cl^- to the dried cit-AgNPs@Ca^{2+}, the resulting spectra resembles the one obtained on the colloidal substrate in the presence of Ca^{2+} and Cl^-, having the distinctive Ag-Cl band (237 cm^{-1}) the most intense feature in the spectrum and Nile Blue signal being selectively enhanced (Figure 3-6 c). This suggests strong binding of Cl^- at the Ag surface for the cit-AgNPs@Ca^{2+} substrate. Based on these experiments, the property of Ca^{2+} to selectively promote the adsorption of anionic species is activated when Ca^{2+} is added to colloidal nanoparticles before the drying process rather than after.

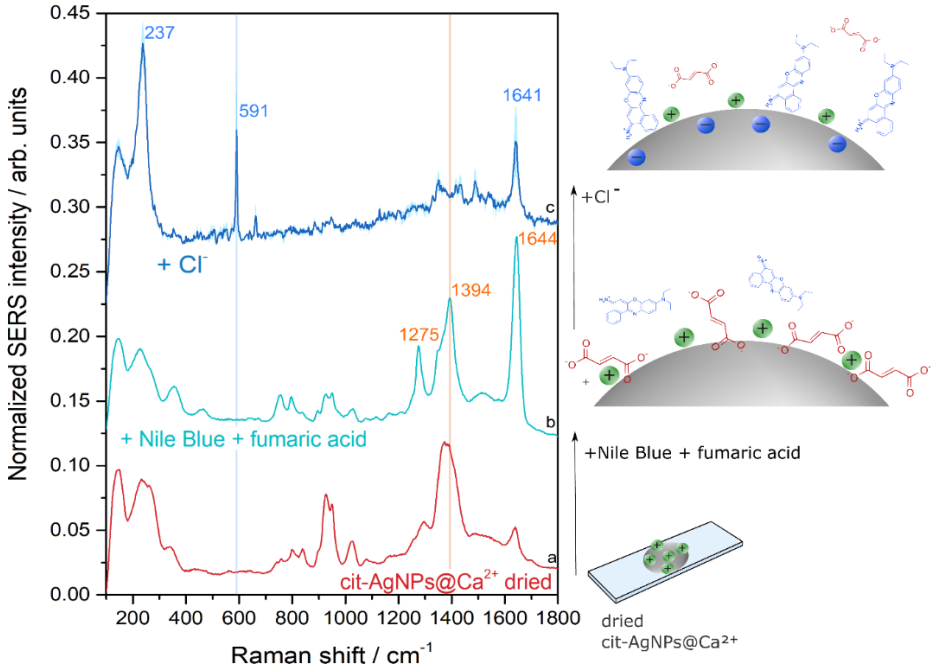

Figure 3-6 SERS spectrum of dried cit-AgNPs@Ca^{2+} substrate (a) submerged in a 50 nM Nile Blue·SO_4 and 5 μM fumaric acid solution (b), SERS spectrum after the addition of 1 mM Cl^- (c). The laser intensity was set at 50%. On the right, the proposed adsorption mechanism on dried Ag surface is schematically shown.

3.4.2 hya-AgNPs@Ca^{2+} for cationic analyte detection

To produce a dried substrate for cationic analyte detection, AgNPs obtained by hydroxylamine hydrochloride reduction (hya-AgNPs) were employed. These nanoparticles were preferred for detecting cationic analytes, having Cl^- ions as their capping agent. Furthermore, they have been used in their colloidal form for obtaining SERS signal from cationic analytes. [17]

First, as-synthesized hya-AgNPs were centrifuged and dried for obtaining a dried substrate (for further details, see Experimental methods). Then, their SERS signal has been tested in the presence of Nile Blue, fumarate, Cl^-, or Cl^- and Ca^{2+}. In all cases, no SERS signal was obtained (Figure 3-7 Left). This suggests that drying as-synthesized hya-AgNPs renders a SERS inactive substrate.

In the case of colloidal hya-AgNPs, Cl^- binds to the surface only in the presence of cations such as Ca^{2+} (Figure 3-7 Right).

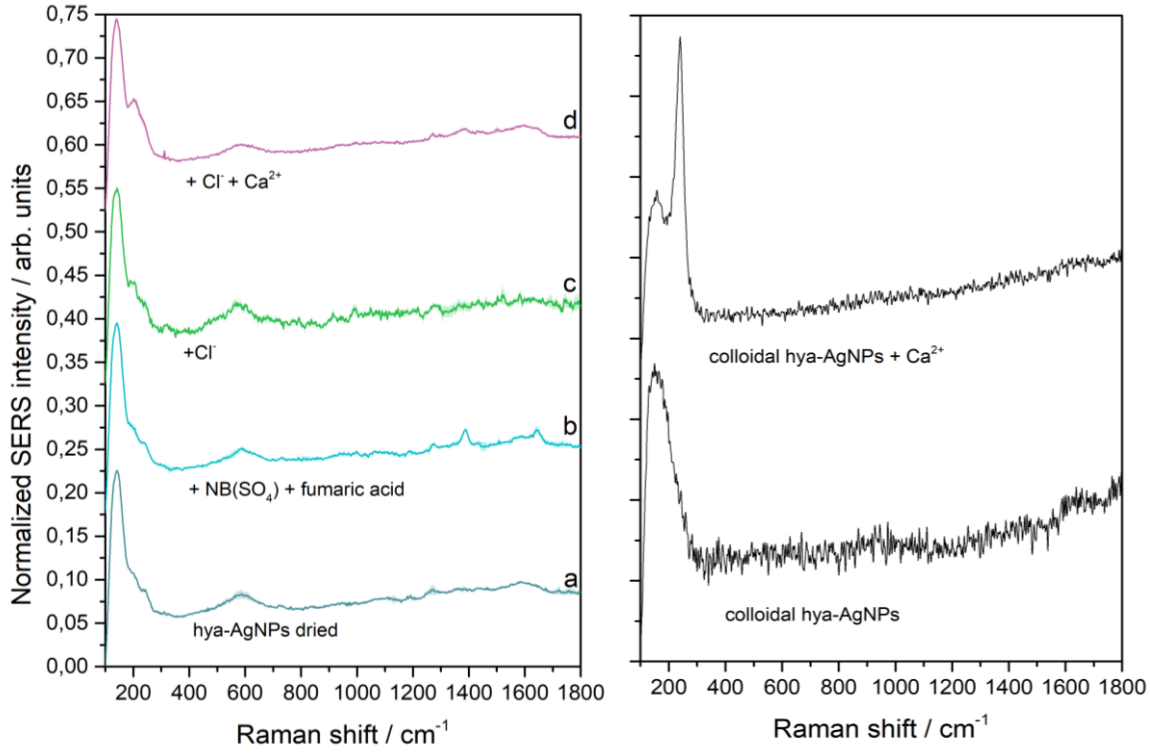

Figure 3-7 Left: *SERS spectrum of a dried hya-AgNPs substrate (a) submerged in a 50 nM Nile Blue·SO_4 and 5 μM fumaric acid solution (b), after the addition of 1 mM Cl^- (c) or 1 mM Cl^- and 0.5 mM Ca^{2+} (d). The spectra exhibit no SERS bands, suggesting no SERS activity of as-synthesized hya-AgNPs after drying.* Right: *SERS spectrum of colloidal, as-synthesized hya-AgNPs exhibiting no SERS bands of the capping agent, similar to cit-AgNPs. The addition of 0.5mM Ca^{2+} to the solution reveals the binding of the capping agent (Cl^-) to the silver surface.*

In line with previous findings, Ca^{2+} was added to the colloidal solution before the centrifugation and drying process. This resulted in a dry SERS active substrate with Cl^- ions adsorbed on the Ag surface, as suggested by the presence of the 235 cm^{-1} peak (Figure 3-8). After adding the mixture of Nile Blue and fumaric acid, the dried hya-AgNPs@Ca^{2+} reveal the selective SERS spectrum of the cationic species, Nile Blue, with no contribution of fumarate. This leads to the conclusion that the addition Ca^{2+} to hya-AgNPs before drying produces a SERS active substrate suitable for direct and selective detection of cationic analytes.

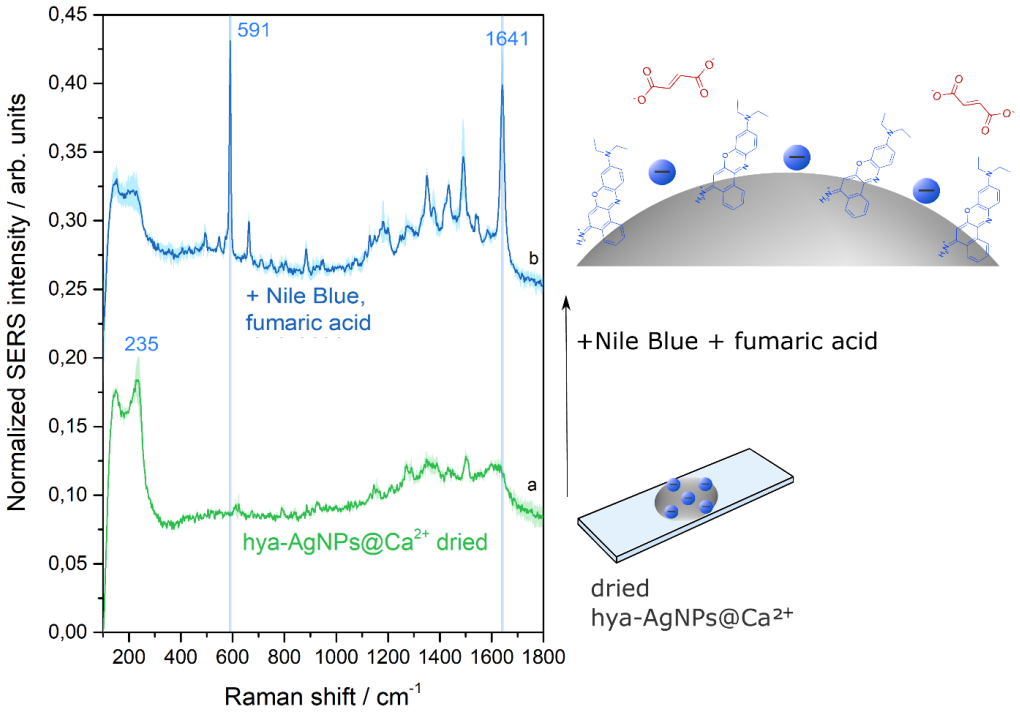

Figure 3-8 SERS spectrum of dried hya-AgNPs@Ca^{2+} substrate (a) submerged in a 50 nM Nile Blue·SO_4 and 5 μM fumaric acid solution (b). The laser intensity was set at 20%. On the right, the proposed adsorption mechanism on dried Ag surface is schematically shown.

3.5 Surfactant-Free SERS substrate

To eliminate surfactant interference altogether, a surfactant-free substrate was developed and optimised, starting from dried cit-AgNPs (see Experimental methods for details).

The optimum duration for ozone exposure, deemed sufficient for the removal of citrate surfactant without reducing the plasmonic properties of AgNPs, was determined to be 7 minutes. SERS spectra confirm that ozone cleaning rendered the substrate SERS inactive, as formation of AgO on the nanoparticle surface occurs (Figure 3-9). Our findings indicate that the most efficient approach of removing AgO from the surface when using H_2O_2 reduction is immersion for 70 seconds in a solution of pH of 4-5. Both solutions result in SERS active substrates, and the spectra confirm effective citrate elimination through this method.

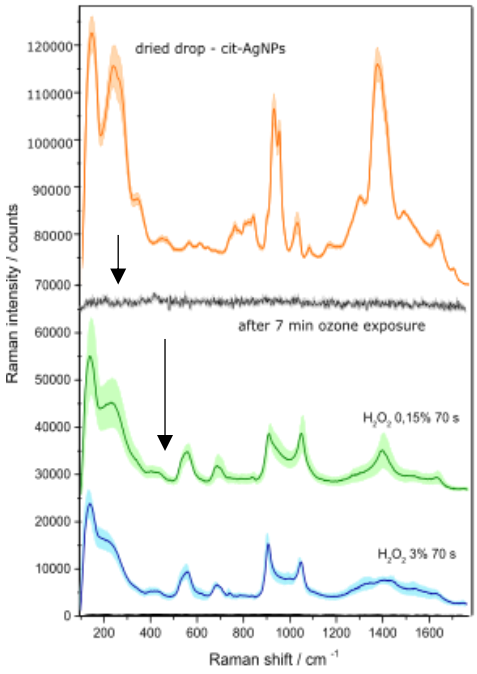

Figure 3-9 Raman spectra of cit-AgNPs: unmodified dried drop exhibiting SERS peaks of citrate (top); dried drop after 7 minutes of UV Ozone Cleaner treatment; dried drop after 7 minutes of O_3 exposure and immersion in H_2O_2 0.15% (green line) and 3% (blue line).

The resulting dried substrate rendered a high SERS signal for the tested analyte, fumaric acid (Figure 3-10). Regarding signal uniformity across the surface, the relative standard deviation (RSD) for the 1275 cm^{-1} peak of fumaric acid was **3.44%** for the 0.15% H_2O_2 protocol, while for the 3% H_2O_2 approach it was **41%**. RSD is the standard deviation of SERS peak intensities relative to their average intensity, typically expressed as a percentage. Values between 5–15% indicate good reproducibility, with exceptional cases reaching 1–3% [27].

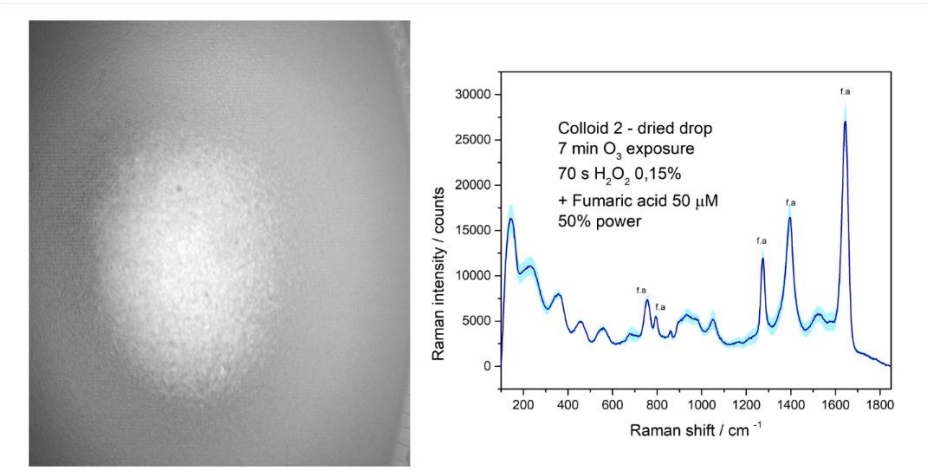

Figure 3-10 Left: microscopical image (20x objective). of a dried drop, after O_3 exposure and H_2O_2 0,15% immersion, showing high nanoparticle density and uniform distribution. Right: average spectrum for 3 points of the same dried drop.

3.6 Optimized SERS detection on a urine sample

To assess whether the optimized cit-AgNPs@Ca^{2+} substrate is suitable for future clinical applications, it was tested on a urine sample from a patient.

First, the influence of pH was evaluated. The dried cit-AgNPs@Ca^{2+} was immersed in 2 mL solution of urine diluted 1:50 in ultrapure water, with a measured pH of 6. As the pH increased, distinct SERS bands started to appear (Figure 3-11 left). The SERS spectrum at pH 10 displays characteristic peaks corresponding to uric acid (636, 806, 1028, 1197, 1358, 1411, 1519, 1548) and creatinine (678, 732, 928) [28], along with an intense peak at 221 cm^{-1}, which decreased in intensity when increasing the pH. Additional measurements at varying sample dilutions showed the dilution of 1:50 to yield the highest SERS signal intensities (Figure 3-11 right).

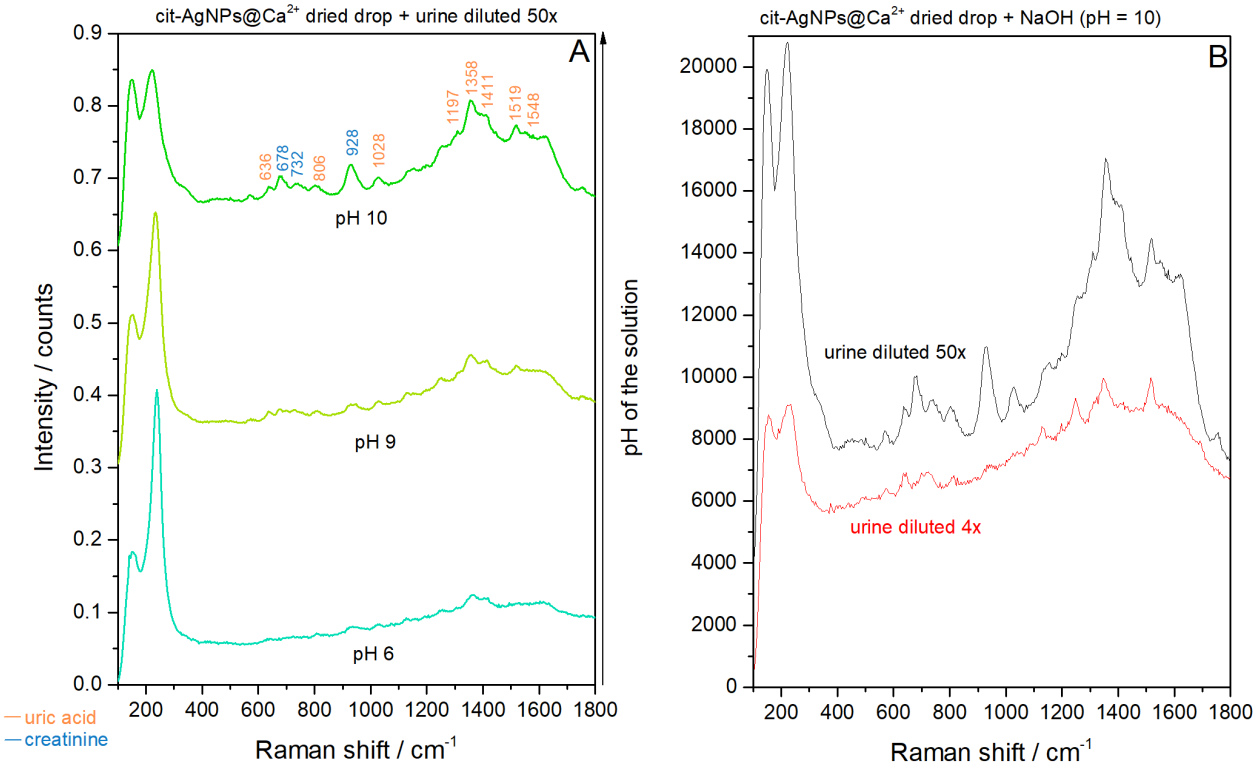

Figure 3-11 SERS spectra of dried cit-AgNPs@Ca²⁺ mixed with urine samples. (A) Influence of urine pH (7, 11, and 12) at 50× dilution. Characteristic bands for uric acid, creatinine, and xanthine are marked. (B) Comparison of spectra at alkaline pH (12) for urine diluted 50× (black) and 4× (red).

Conclusions

In this work, two solid SERS substrates were developed for the selective detection of anionic and cationic analytes. The role of ions such as Ca^{2+} and Cl^- was crucial, highlighting their importance in enabling selective SERS detection in both colloidal systems and dried nanoparticle substrates. It was demonstrated that Ca^{2+} must be introduced prior to the drying process in order to influence the surface potential effectively; once dried, the addition of Ca^{2+} no longer contributes to selectivity.

The **dried cit-AgNPs@Ca^{2+}** was optimized for selective anionic detection, while **dried hya-AgNPs@Ca^{2+}** successfully enabled selective detection of cationic analytes, exploiting the presence of Cl^- ions on the surface from synthesis process.

Additionally, a straightforward two-step method was developed to produce a **surfactant-free substrate** starting from dried cit-AgNPs. This involved first removing the surfactant via ozone exposure, followed by mild chemical reduction to eliminate the resulting silver oxide layer. The resulting substrate provided a strong and uniform SERS signal for fumaric acid, achieving an RSD of just 3.44%, thus demonstrating excellent SERS performance.

Finally, the dried cit-AgNPs@Ca^{2+} substrate was validated in a **real biological matrix**, a urine sample from a patient. The substrate performed best for a 1:50 sample dilution and for a pH of 10, successfully enabling the detection of uric acid and creatinine. Given that creatinine is commonly used as an internal reference in clinical biomolecular quantification, this result highlights the potential of the substrate for clinical implementation. Further measurement protocol and substrate optimisation may enhance its performance for biofluid analysis and extend its diagnostic applications.

References

[1] A. Otto, A. Bruckbauer, and Y. X. Chen, *On the chloride activation in SERS and single molecule SERS*, Journal of Molecular Structure, **661–662**, pp. 501–514, 2003.

[2] E. C. Le Ru and P. G. Etchegoin, *Principles of surface-enhanced Raman spectroscopy : and related plasmonic effects*. Amsterdam ; Boston : Elsevier, 2009. [Online]. Available: http://lib.ugent.be/catalog/rug01:001875827

[3] A. Stefancu, S. D. Iancu, and N. Leopold, *Selective Single Molecule SERRS of Cationic and Anionic Dyes by Cl– and Mg2+ Adions: An Old New Idea*, J. Phys. Chem. C, **125**, no. 23, pp. 12802–12810, 2021.

[4] L. R. Terry, S. Sanders, R. H. Potoff, J. W. Kruel, M. Jain, and H. Guo, *Applications of surface-enhanced Raman spectroscopy in environmental detection.*, Anal Sci Adv, **3**, no. 3–4, pp. 113–145, 2022.

[5] G. Xu, P. Song, and L. Xia, *Examples in the detection of heavy metal ions based on surface-enhanced Raman scattering spectroscopy*, Nanophotonics, **10**, no. 18, pp. 4419–4445, 2021.

[6] V. Moisoiu *et al.*, *SERS liquid biopsy: An emerging tool for medical diagnosis*, Colloids and Surfaces B: Biointerfaces, **208**, p. 112064, 2021.

[7] A. Stefancu *et al.*, *SERS-based liquid biopsy of saliva and serum from patients with Sjögren's syndrome.*, Anal Bioanal Chem, **411**, no. 22, pp. 5877–5883, 2019.

[8] C. D. Bocsa, V. Moisoiu, A. Stefancu, L. F. Leopold, N. Leopold, and D. Fodor, *Knee osteoarthritis grading by resonant Raman and surface-enhanced Raman scattering (SERS) analysis of synovial fluid.*, Nanomedicine, **20**, p. 102012, 2019.

[9] S. D. Iancu, A. Stefancu, V. Moisoiu, L. F. Leopold, and N. Leopold, *The role of Ag+, Ca2+, Pb2+ and Al3+ adions in the SERS turn-on effect of anionic analytes*, Beilstein J. Nanotechnol., **10**, pp. 2338–2345, 2019.

[10] J.-A. Huang, Y.-L. Zhang, H. Ding, and H.-B. Sun, *SERS-Enabled Lab-on-a-Chip Systems*, Advanced Optical Materials, **3**, no. 5, pp. 618–633, 2015.

[11] D.-B. Grys *et al.*, *Controlling Atomic-Scale Restructuring and Cleaning of Gold Nanogap Multilayers for Surface-Enhanced Raman Scattering Sensing.*, ACS Sens, **8**, no. 7, pp. 2879–2888, 2023.

[12] *Survey of Light-scattering Phenomena*, in *The Raman Effect*, John Wiley & Sons, Ltd, 2002, pp. 3–18.

[13] P. J. Larkin, *Chapter 2 - Basic Principles*, in *Infrared and Raman Spectroscopy (Second Edition)*, Second Edition., P. J. Larkin, Ed. Elsevier, 2018, pp. 7–28.

[14] M. Fleischmann, P. J. Hendra, and A. J. McQuillan, *Raman spectra of pyridine adsorbed at a silver electrode*, Chemical Physics Letters, **26**, no. 2, pp. 163–166, 1974.

[15] S. A. Maier, *Enhancement of Emissive Processes and Nonlinearities*, in *Plasmonics: Fundamentals and Applications*, New York, NY: Springer US, 2007, pp. 159–176.

[16] A Otto, I Mrozek, H Grabhorn, and W Akemann, *Surface-enhanced Raman scattering*, Journal of Physics: Condensed Matter, **4**, no. 5, p. 1143, 1992.

[17] N. Leopold *et al.*, *The role of adatoms in chloride-activated colloidal silver nanoparticles for surface-enhanced Raman scattering enhancement*, Beilstein J. Nanotechnol., **9**, pp. 2236–2247, 2018.

[18] C. Eggeling *et al.*, *Homogeneity, Transport, and Signal Properties of Single Ag Particles Studied by Single-Molecule Surface-Enhanced Resonance Raman Scattering*, J. Phys. Chem. A, **105**, no. 15, pp. 3673–3679, 2001.

[19] A. Stefancu, S. D. Iancu, V. Moisoiu, and N. Leopold, *Specific and Selective SERS Active Sites Generation on Silver Nanoparticles by Cationic and Anionic Adatoms*, Rom Rep Phys, **70**, 2018.

[20] M. Niihori *et al.*, *SERS Sensing of Dopamine with Fe(III)-Sensitized Nanogaps in Recleanable AuNP Monolayer Films*, Small, **19**, no. 48, p. 2302531, 2023.

[21] H. Qayyum *et al.*, *Laser synthesis of surfactant-free silver nanoparticles for toxic dyes degradation and SERS applications*, Optics & Laser Technology, **129**, p. 106313, 2020.

[22] P. C. Lee and D. Meisel, *Adsorption and surface-enhanced Raman of dyes on silver and gold sols*, J. Phys. Chem., **86**, no. 17, pp. 3391–3395, 1982.

[23] N. Leopold and B. Lendl, *A New Method for Fast Preparation of Highly Surface-Enhanced Raman Scattering (SERS) Active Silver Colloids at Room Temperature by Reduction of Silver Nitrate with Hydroxylamine Hydrochloride*, J. Phys. Chem. B, **107**, no. 24, pp. 5723–5727, 2003.

[24] Y. Zhang, S. Prabakar, and E. C. Le Ru, *Coadsorbed Species with Halide Ligands on Silver Nanoparticles with Different Binding Affinities*, J. Phys. Chem. C, **126**, no. 20, pp. 8692–8702, 2022.

[25] D. Paramelle, A. Sadovoy, S. Gorelik, P. Free, J. Hobley, and D. G. Fernig, *A rapid method to estimate the concentration of citrate capped silver nanoparticles from UV-visible light spectra*, Analyst, **139**, no. 19, pp. 4855–4861, 2014.

[26] M. Nara, H. Torii, and M. Tasumi, *Correlation between the Vibrational Frequencies of the Carboxylate Group and the Types of Its Coordination to a Metal Ion: An ab Initio Molecular Orbital Study*, J. Phys. Chem., **100**, no. 51, pp. 19812–19817, 1996.

[27] D.-B. Grys, R. Chikkaraddy, M. Kamp, O. A. Scherman, J. J. Baumberg, and B. de Nijs, *Eliminating irreproducibility in SERS substrates*, Journal of Raman Spectroscopy, **52**, no. 2, pp. 412–419, 2021.

[28] D. Andras *et al.*, *Advancing Breast Cancer Diagnosis: Optimization of Raman Spectroscopy for Urine-Based Early Detection*, Biomedicines, **13**, no. 2, 2025.

Anexa 2

DECLARAȚIE PE PROPRIE RĂSPUNDERE

Subsemnata, **Ion Georgiana**, declar că **Lucrarea de disertaţie** pe care o voi prezenta în cadrul examenului de finalizare a studiilor la **Facultatea de Fizică**, din cadrul Universităţii Babeş-Bolyai, în sesiunea **iulie 2025**, sub îndrumarea **prof. dr. Nicolae Leopold**, reprezintă o operă personală. Menţionez că nu am plagiat o altă lucrare publicată, prezentată public sau un fişier postat pe Internet. Pentru realizarea lucrării am folosit exclusiv bibliografia prezentată şi nu am ascuns nici o altă sursă bibliografică sau fişier electronic pe care să le fi folosit la redactarea lucrării.

Prezenta declaraţie este parte a lucrării şi se anexează la aceasta.

Data,

23.06.2025

Nume,

Ion Georgiana

Semnătură